Geomatica 76 (2024) 100019

Contents lists available at ScienceDirect

Geomatica

journal homepage: www.sciencedirect.com/journal/geomatica

Assessment of active tectonics of the Tripura-Mizoram fold belt (Surma Basin), North East India

Mery Biswas [a], Soumyajit Mukherjee [b,*], Manash Pratim Gogoi [c], Nabanita Barik [b]

[a] Department of Geography, Presidency University, Kolkata, West Bengal, India
[b] Department of Earth Sciences, Indian Institute of Technology Bombay, Powai, Mumbai Maharashtra, India
[c] Department of Geology, Sibsagar College, Joysagar, Sivasagar, Assam, India

ARTICLE INFO

Keywords:
Tectonics
Geomorphic indices
Well-bore stability
Active tectonics
NE Himalaya

ABSTRACT

The Tripura-Mizoram fold belt is situated in the north-eastern part of India. Northeastern Himalaya including this region is tectonically very active, partly petroliferous, and has international attention from academicians and industry persons. This study aims at locating areas of recent tectonic vulnerability. Drainage networks are proxies of active faulting. Changes in geomorphic indices e.g., long profile analysis, basin-scale parameters, stream length gradient index and steepness index along the rivers in the eighteen watersheds extracted within the study area are evaluated. The Index of active tectonics (IAT) derived from the basin-scale parameters is classified into five classes: Class 1 (IAT =1.875–2.000), Class 2 (IAT = 2.001-2.375), Class 3 (IAT = 2.376-2.750), and Class 4 (IAT = 2.751-3.250) and Class 5 (IAT = 3.000-3.320). Class 1 indicates the highest activity of tectonics. The tectonic sensitivity is also marked in micro-scale where rivers cross lineaments / faults. Elevations from source to mouth of individual consequent rivers of each watershed indicate the most vulnerable sections where the channels run along and across the faults or lineaments in watersheds 2, 14 and 15. The computed R^2 values and the IAT identify watershed 2 and watershed 15 as the tectonically most active. Well-bore stability issue from the Petroleum mining lease (PML) blocks needs to be taken care from watershed 2, 3 and 15.

1. Introduction

Neogene Surma tectonic watersheds comprise of a belt of regional folds with marked sub-meridian trend and arcuate shape with westward convexity (Nandy, 1982). The Surma basin consists of N-S trending folds due to E-W compression, along with westward-convexing. Ridges and valleys define the first-order topography of the basin. The basin has NE- and NW-trending lineaments and (strike-slip conjugate) faults [38]. According to Ganguly [17], the asymmetric anticlines of Tripura –Mizoram fold belt is separated by open synclines, which deformed progressively towards west [33]. During the Middle Eocene to Early Miocene, collision between the Indian and the Burmese/Mayanmar plate led to thick sedimentation at the west of the Indo-Mayanmar range. The uplifted Tripura-Mizoram fold belt comprises of several tectonic episodes through four stages- synrift and pre-collision, drifting of sediments, early collision and late collision [10]. Recent fieldworks and analogue models indicate that the belt is mechanically weak and brittle deformed [13]. The shallow marine deltaic sediments form the Surma Group crop out as the Tripura –Mizoram fold belt in terms of Sitapahar anticline, Rangamati area and the Mirinja anticline [3,4,32,31,33,39]. Most of the Mizoram fold belt is composed of Neogene sandstone over shale/siltstone of the Bhuban Formation. The region experienced two major earthquakes in 1897 and 1950 (Mw $\geq$ 8.0) [20]. Seismologically this fold belt is very active due to the dextral-slip of the plate wedge along the Indo–Burma Arc [20]. The area has remained active during 1969–2012 when several smaller seismic events happened [14].

Morphometry is a quantitative tool that can decipher active tectonics (review in [46]). Entrenched river channels with incision processes and geometric characters of channel orientation reveal the role of tectonic geomorphology in assessing active tectonics in the watershed-scale. It also helps in evaluation of geometric characteristics of the fluvial landscape [47]. Accelerated tectonic deformation resulted in topographic development in terms to tilting, incision, migration and asymmetry of the watersheds [48].

The emerging trends in the space technology and applications of spatial data become very useful for surface characterization, interpretation and management of the quantitative data sets review in [16]). In the Indian scenario, morphotectonic analysis has been implemented for

* Corresponding author.
E-mail addresses: smukherjee@iitb.ac.in, soumyajitm@gmail.com (S. Mukherjee).

https://doi.org/10.1016/j.geomat.2024.100019
Received 7 April 2024; Received in revised form 29 July 2024; Accepted 11 August 2024
Available online 21 August 2024

several purposes especially for watershed analysis and prioritization of micro watersheds [18,7,8]. Drainage system adjusts to any modifications in surface morphology and any structural deformations.

Ibotombi and Singh [24] discussed centripetal and centrifugal drainage patterns and structural controls from the Manipur state. These authors did not perform any morphometric analysis from the terrain. Rakshit and Bezbaruah [41] performed a morphometric analysis around Aizawal. The work lacks regional significance. On other hand, even though Barman et al. [2] undertook a morphometric study of a part of the present study area. They deduced morphometric parameters some of which are same as this work. But whether these were done on meso- or micro-scale was not stated. In contrast, the present study area covers a much larger terrain than Barman et al. [2] (Fig. 1) and we find out morphometric parameters on micro-scale. The index of active tectonics (IAT) [34] is utilized in this work to classify the watersheds as a measure of active tectonic magnitude as low to very high.

Two major factors that modulate river incision rates are climate and tectonics. In a steady state condition, when uplift rate balances the erosion rate, the longitudinal profile of a river becomes graded [41]. Landscape deformation is well connected with the structure and lithology of terrains. Here the elongated fold belts of shales and siltstones are well jointed [9]. The low cohesion resulting in slope instability [9] and the parallel drainage system [9] with elongated watersheds in Mizoram fold area set scopes for morphotectonic studies along with Triputa fold belt under Surma basin.

Within 1964–2011, total 1579 earthquakes have been recorded between 4 to 7.9 Mb. Previous earthquake analysis from the area was based on magnitude ranges for a particular time span as 1965–2006. However, frequency/ magnitude analysis based on 'b-value' remained a due from the study area. Such a work was undertaken form the western Himalaya by Kothyari et al. [29]. Seismic tremor is one of the factors that control geomorphology [49]. Endogenic tectonic processes, on the other hand, positively build the landscape and are primarily structure-controlled. Along stacked imbricate thrusts, the Indo-Mayanmart fold and thrust belt actively overthrust the Indian continental basement and its Palaeogene–Neogene crust to the east, resulting in shallow and moderate-depth earthquakes [37].

The Surma basin and in fact the entire study area is important from the perspective of hydrocarbon exploration [27]. A part of the study area comes under the *"Category IIID: Tripura-Mizoram forearc basin"* defined within an orogenic setting [15]. Already there are 14 Petroleum Mining Lease (PML) in the area. Thus, this work has two objectives:

- Spatial and linear-scale analysis of 18 watersheds of the fold belt to determine active tectonics
- Seismological study to investigate the active tectonics

2. Geology

The Surma Group of Mio-Pliocene rocks are overlain unconformably by the Oligocene Barail Group. Ancient Surma deposits are found in Tripura's central and eastern regions, while the younger Tipam Group crops out in the western region. The upper and lower portions of the Bhuban Formation are primarily arenaceous, whereas the mid-part is primarily argillaceous (Samal 2017). After a spatially widespread post-Barail pause, at the end of the Oligocene, the Surma sediments were laid down over the Barails or coeval rocks in the Surma valley, south of the Shillong plateau.

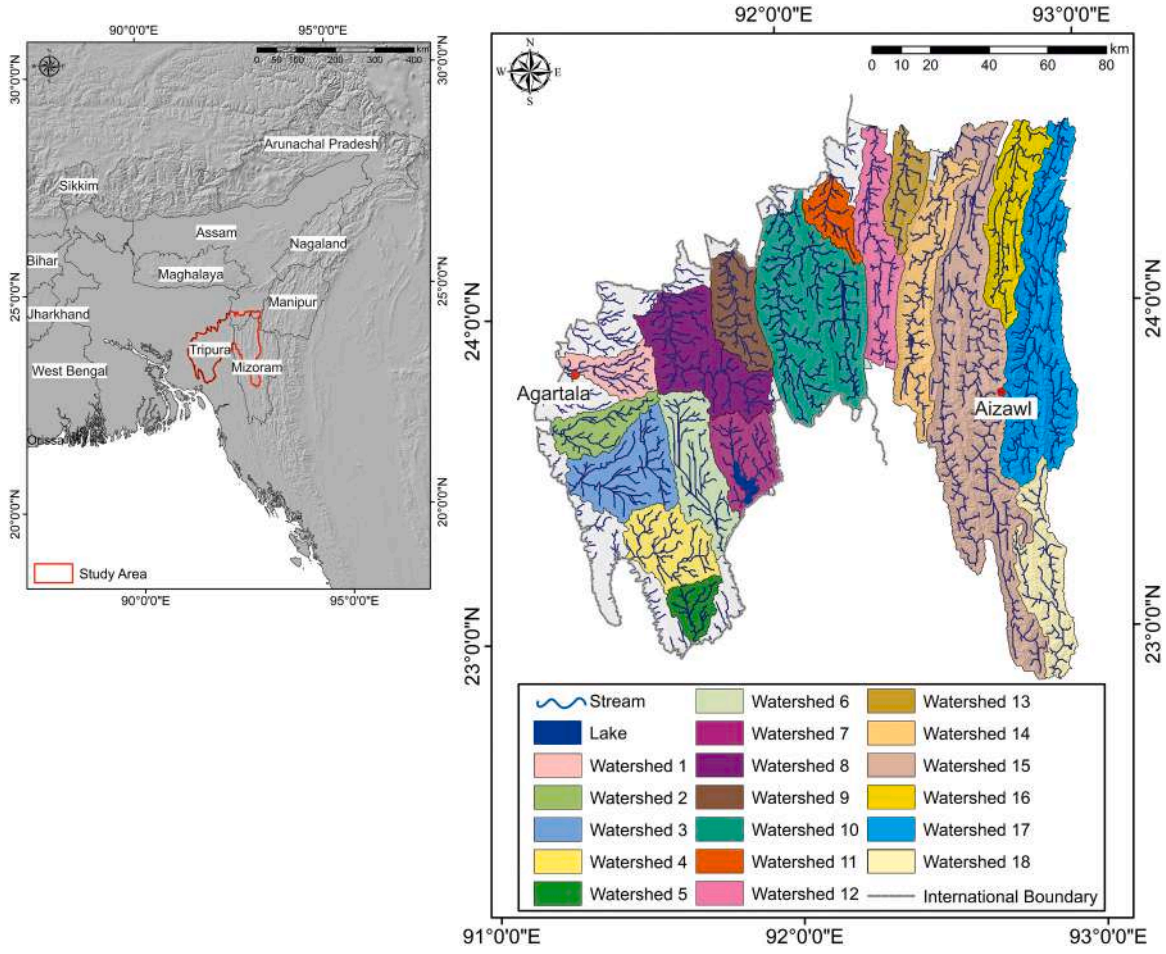

Fig. 1. Study area with 18 delineated watersheds within the Tripura –Mizoram fold belt.

Most transverse faults follow one of these trends: NE-SW, ENE-WSW and NW-SE. The NW-trending Mat river fault/ Mat Fault, which runs through Mizoram between Aizawl and Lunglei, is the most significant transverse fault with a dextral-slip. NW-SE trending Gomti/Gumti Fault crossed the watersheds 6, 7, 10, 14, 15, 16 and 17. Possibly, only the deeper part of the Mat Fault is undergoing slip [53]. The fault has been active neotectonically as has been revealed by radon/thoron concentration [25,26,52]. The fault governs geomorphology to some extent as found from the Mat river course that locally follows this fault [25]. However, not all seismicity around the Mat Fault is related to the fault's activation (e.g., [35]). Seismicity could also be related to the secondary faults associated with the Mat Fault [40]. The Chite Fault near Aizawal revealed radon concentration in sub-surface [43]. This indicates that the fault is active. NE-SW trending transverse lineaments pass through areas of axial depressions and culminations as well where fold axes abruptly change trends [41]. Long arcuate linear folds in the Surma basin was layer-parallel compressed along E-W. This statement however contradicts many researchers [17] that the terrain underwent vertical tectonics [41].

The most recent significant earthquake was recorded in 2015 (https://www.usgs.gov/programs/earthquake-hazards/data). As per the cumulative earthquake rate, and the curve distribution of earthquake depth and magnitude shows that multiple recent seismic occurrences with the maximum magnitude and depth between 2010 and 2020. (Fig. 2a-d). Thuamthansanga et al. (2008) studied the b-values from the study area. They analysed both 'a' and 'b' value based on the 1965–2006 seismic data set. However, they missed the issues of morphotectonic signatures and active tectonics with respect to drainage pattern configuration.

3. Data acquisition & methods used

3.1. Meso-scale data

We used NASA's Earth Data (2021) and the mosaicked scenes of the Digital Elevation Model (DEM)—Shuttle Radar Topography Mission (SRTM) with 1 arc-second (~ 30 m) resolution. The drainage watersheds were generated using the D8flow algorithm in the ArcGIS10.4 (Esri 1999) platform. All the geomorphic indices and metadata for the sub-watersheds and the final maps were prepared in ArcGIS10.4 (Esri 1999).

The stream networking system reflects the control of shorter lineaments and faults as well the slope direction. The index of active tectonics (IAT) [36] has been calculated using the parameters - Basin shape Index (B_s), Form Factor (Rf), Hypsometric Integral (HI), Circularity Ratio (R_c), Elongation Ratio (R_e), Transverse Topographic Symmetry (T), Asymmetry Factor (AF) and Drainage Texture (Dt) (Table 1). Active tectonic has been assessed using spatial-scale parameters (Supplementary Figs. 1a-h).

3.2. Micro-scale data

For micro-scale watershed analysis, satellite-based remote sensing

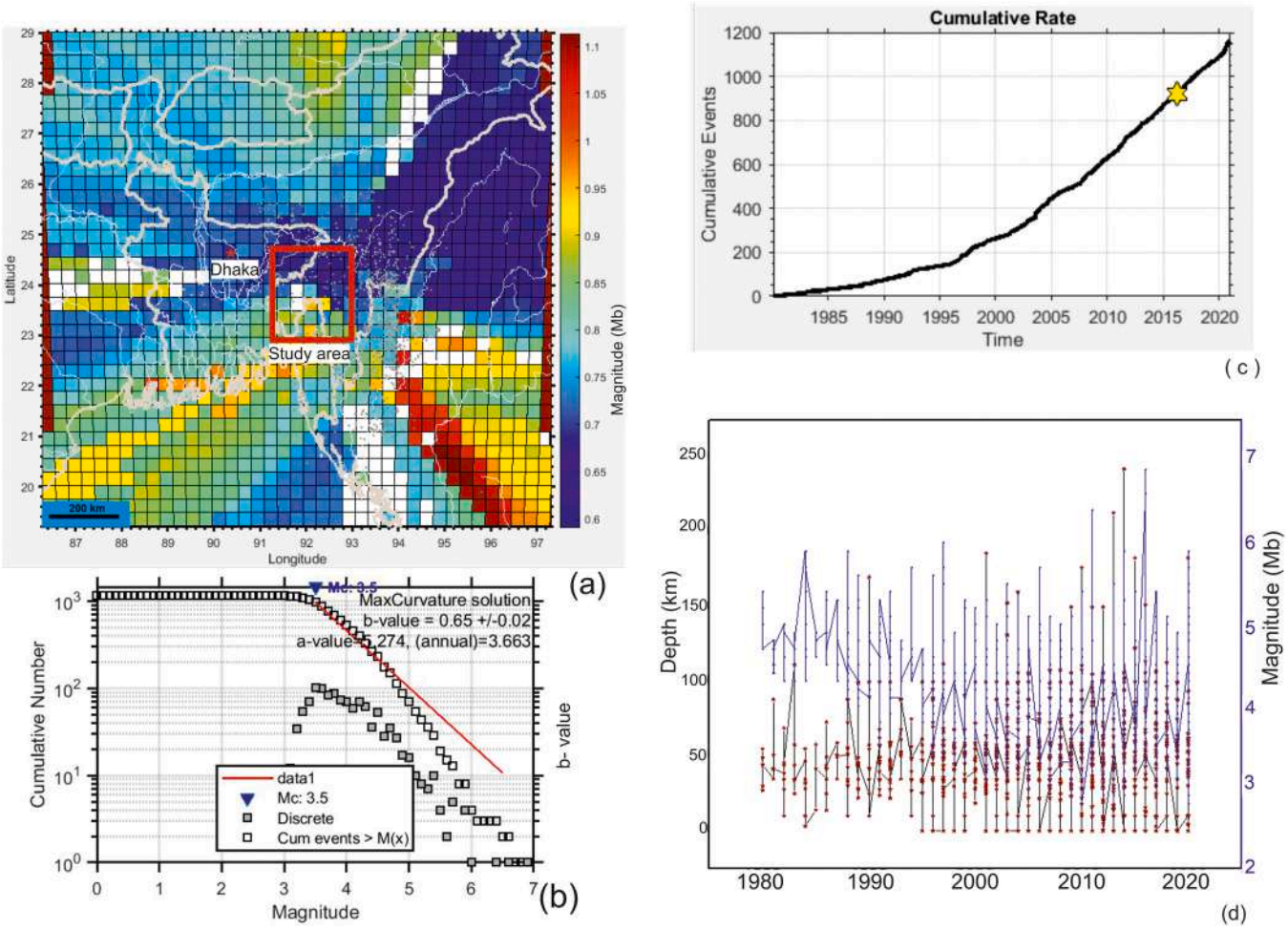

Fig. 2. a. Showing spatial variation in b-value across the entire NE India extended from 86° E- 88° E and 19 °E-29 °E. **b.** Temporal variation in cumulative number of seismic events. **c.** Graphical presentation of time-specific cumulative events of earthquake with a major event in 2015. **d.** Magnitude (Mb) vs. depth (km) distribution for the 1980–2020 events.

Table 1
Indicators for morpho-tectonic analysis.

Sl. No.	Formula for basin scale indicators (unitlesss)	Equations & meaning of symbols	Explanations	References
1.	**Hypsometric integral** (HI)	$\frac{(Ele_{avg} - Ele_{min})}{(Ele_{max} - Ele_{min})}$ Ele_{avg}: Average of elevation Ele_{min}: Minimum elevation Ele_{max}: Maximum elevation	The hypsometric integral is a dimensionless number that allows different sub-basins to be compared regardless of the scale. Hypsometric Integral indicates both tectonic activeness and lithological control. The rate of relief uplift is positively correlated with the hypsometric integral. HI value varies between 0 and 1 and a value nearer to 1 indicate a tectonically very active basin, 0.5 HI value is an indicator of equilibrium (mature) state and a value nearer to 0 indicates tectonically less active basin. To simulate the geological phases in the development of a watershed, hypsometric integral is one of the indicators that specify the tectonics. It has generated in respect of a particular drainage basin using relative drainage basin height (h/H) that is known as the total basin height ratio against the relative drainage basin area (a/A) which is the total basin area ratio[28]. Maximum range of Hi values are indicative of the development of recent landforms resulted from active tectonics (Hamdouni et al., 2008).	Strahler[45], Schumm (1956) Andreani et al. (2014)
2.	**Elongation fatio** (R_e)	$Re = 1.128\sqrt{\frac{A}{L_b}}$ A: signifies the area of the basin, Lb: denotes the length of the basin.	Elongation ratio is influenced by geology and climate. The values vary from 0 to 1 (e.g. Wołosiewicz, 2018). As the landscape evolves, the river basin becomes circular and the value tends to be 1.	Schumm (1956); e.g. Wołosiewicz (2018)
3.	**Circularity ratio** (R_c)	$Rc = \frac{4\pi A}{P^2}$ P: indicates the perimeter of river basin; A: signifies the area of the basin	Circularity ratio of the river basin is influenced by the geologic structures, stream length and frequency, slope and climate. High values indicate the circular shape of the basin indicating the landscape to be mature. Unit circularity ratio (R_c) depicts a watershed's circular shape and indicates uniform infiltration with a long delay before the water's surplus reaches the outlet or confluence, which is further dependent on the geology, slope and land cover (Reddy et al.2004).	Horton[23]
4.	**Asymmetry factor** (AF)	$AF = \left(\frac{A_r}{A_t}\right)*100$ A_r: area of the basin (km^2) to the right of the main channel facing downstream and A_t: total area (km^2) of the basin.	An indicator to measure how much a river basin is tilted due to tectonics. Tectonic activity causes the main stream to change course, sloping away from the basin's midline. The asymmetry factor depicts the relationship between tectonic tilt in watersheds[28]. Anand and Pradhan 2018 calculated the normalized AF deducting the actual value from 50.	Hare & Gardner (1985); e.g. Anand & Pradhan (2019)
5.	**Form factor** (R_f)	$R_f = \frac{A_B}{(L_b)^2}$ Rf value varies between 0 and 1. When this value is near to 0, the basin is supposed to be tectonically active, while as the value approaches towards 1, the tectonic activeness decreases correspondingly.	The form factor (R_f) determines the ratio of watershed area to square of the watershed length[22]. The form factor (R_f) determines the ratio of watershed area to square of the watershed length[22]. The form factor (R_f) is defined as the ratio of the watershed area to the square of the watershed length.	Horton[22]
6.	**Drainage texture (D_t)**	$D_t = Nu/P$ Nu: Number of streams of a given order. P: Perimeter (km) of the watershed	The underlying lithology, infiltration potential, and relief characteristics of the terrain all affect drainage texture. Dt is the total number of stream segments in all orders along the watershed's edge[23]. This is the relative channel spacing in fluidly prepared terrain, depending on many natural factors such as climate, precipitation, vegetation, rock / soil type, permeability, undulations, and watershed development stages (Kale and Gupta 2001). On the other hand, T is the product of Dd and F. It is calculated by multiplying the	Horton[23]

(*continued on next page*)

Table 1 (*continued*)

Sl. No.	Formula for basin scale indicators (unitlesss)	Equations & meaning of symbols	Explanations	References
			drainage density by the current frequency. If less than 4, T is classified as a coarse drainage texture. Intermediate drainage structure if it is between 4 and 10; fine drainage structure if it is between 10 and 15; ultrafine drainage structure if it exceeds 15. (Smith 1950).	
7.	**Transverse topographic symmetry** (T)	$T = \frac{Da}{Dd}$ Da: the distance from the drainage basin's midline to the meander belt's midline Dd: the distance from the basin's midline to the basin divide.	'T′ in a perfectly symmetric basin has a value of zero. As asymmetry develops, 'T′ likewise rises and eventually reaches a value of one. For various lengths of stream channels, the transverse topographic symmetry factor is computed and reveals the stream's preferred migration direction perpendicular to the drainage axis. It is a reconnaissance tool for any area, presenting lateral tilting due to tectonics (Cox et al., 2008). The computed values of 'T′ construe the cause of asymmetry, which could depend on change in lithology and structural during the tectonic events and it disclose the neotectonic activity.	Cox (1994), Sajadian et al., (2015), Takieh (2015)
8.	**Basin shape index** (Bs)	$Bs = \frac{Bl}{Bw}$ Bl: measured length from headwater to the point on the mouth of the basin, Bw: measured width at the widest point on the basin.	Watersheds that are relatively young in term s of active tectonics can be constrained in terms of watershed shape index (Bs). A basin parallel to the terrain slope indicates that it is structurally active. The width of the basin is reduced and the energy of the flow develops through vertical incisions, mainly near areas of active crustal movement in upper Bhuban Fm and middle Bhuban Fm of Mizoram fold belt (Lokhoet al., 2016). In contrast, rapid uplift is confused where the valley extends due to lateral erosion on less active flat terrain, which is common in the lower reaches of lower slopes.	Bull and McFadden [12]; Ramirez-herrera (1998)
9.	**Valley floor width height ratio (Vfwh)**	$Vfwh = \frac{2V_{fw}}{[(E_{ld} - E_{rd}) + (E_{rd} - E_{sc})]}$ Here *Vf* w: width of the valley floor, E_{ld} and E_{rd}: elevations of the divide on the left and right side of the valley, respectively. *Esc*: average elevation of the valley.	This index distinguishes between small, steep valleys with a "V" form and large valleys with a "U" shape relative to the height of valley dividers. In general, valleys with a U form have high values of V_f, whereas valleys with a V shape have relatively low values. Since uplift and incision go hand in hand, the index is thought to be the driving force behind dynamic tectonics, where low V_f values are linked to higher rates of both uplift and incision. In an equilibrium state, incision and uplift are almost coordinated, although this index may be a measure of incision rather than uplift. Valley floor to height ratio (Vfwh)[12] shows the localised conditions of the channel, which depends on presence of resistant rocks or due to the presence of structural feature. A drainage watershed that has experienced progressive upliftment will develop prominent valley profiles. Watersheds having wide and flat valleys possess higher values of Vfwh in contrast to valleys experiencing rapid incision by stream erosion.	Bull and McFadden[12]
Sl. No.	**Linear-scale indicators**	**Equations & meaning of symbols**	**Explanations**	**Reference**
1.	Sinuosity Index (SI)[unitless]	$SI = \frac{CL}{Vl}$ CL: channel length between two points on a river, *Vl*: the valley length.	Sinuosity, a measure of a channel's degree of meandering, used to identify the different geomorphological river types.	Brice[11], Schumm and Khan (1972), Biswas and Dhara (2019)
2.	Channel Concavity (ɵ)[in degree]	$Ceh = 1/(S2 - S1)\triangle ES$: Where, S1 is the channel slope prior to disturbance, S2 is the channel slope after disturbance (e.g. due to a change in incision rate E) and $\triangle E$ is the difference between the incision rate before and after disturbance.	Channel concavity explain the differential rates of uplift and erosion. The concept developed as a relationship between slope and area. Whipple (2004) categorized concavity (ɵ) into four types: i) low concavity (< 0.4) is related to short, steep	Wobus et al. (2006), Whipple et al. (2007)

(*continued on next page*)

Table 1 (*continued*)

Sl. No.	Formula for basin scale indicators (unitlesss)	Equations & meaning of symbols	Explanations	References
			drainage dominated by debris flow, ii) moderate concavity (0.4 −0.7) is associated with actively uplifting bedrock channel, iii) high concavity (0.7 −1) is related to decrease in the uplift, and iv) extremely high concavity (> 1) denotes a transition from incisive to depositional conditions	

study of surface features [6,50,54] and Digital Elevation Model (DEM) based GIS study of landforms [44] provide quantitative analyses of geomorphic study [42].

Vector file of the Indian administrative boundaries (published in January 2018) has been collected from the ArcGIS Hub (URL: https://hub.arcgis.com; accessed on 17-Jan-2021) to extract the boundary of study area. Landsat OLI 8 data of the study area was taken from the United States Geological Survey (USGS) – EarthExplorer (URL: https://earthexplorer.usgs.gov; accessed on 07-Aug-2021). We took Carto DEM version 3 R1 of Cartosat 1 from Bhuvan Data Archive of National Remote Sensing Centre (NRSC) from the URL: https://bhuvan-app3.nrsc.gov.in/data/download/index.php, accessed on 07-Aug-2021. GIS software viz. QGIS and Global Mapper were used to perform DEM and raster-based analyses. Vector layers of drainage and lineaments were acquired using the digitiser tools. In-built raster tools were used to perform profile analyses, ridge (lineament) mapping, drainage analyses and hypsometric curves were generated. Spreadsheet of Excel 2020 was used to perform statistical calculations e.g., linear, exponential, logarithmic and power regression. We analysed the hypsometric curves [45] by using percentage method with two parameters-(a/A) and (h/H). Here a: area of two given contours, A: total area, h: elevation of that contour above the lowest point in the basin, and H: relief of the basin.

3.3. Seismic data analysis

The 50 years of seismicity data from 1970 to 2020 considered for the study is in homogeneous body wave magnitude scale (Mb) as per the catalogue of the International Seismological Centre's (IRIS) Incorporated Research Institutions for Seismology, Advanced National Seismic System (ANSS), and United States Geological Survey (USGS). The data is taken from the region bounding between 19° N to 29° N latitudes, and 85° E to 93° E longitudes. The earthquake catalogues was processed and used for the seismic analysis using the Z-Map 7.1 software (2018), compatible with MATLAB 18 version (2018).

The Frequency-Magnitude Distribution (FMD), also known as Gutenberg-Richter Relationship (Gutenberg and Richter 1944, 1954), describes the number of earthquakes (N) as a function of their magnitude (M):

$$\log N = a - b\,M \quad (1)$$

N: cumulative number of earthquakes of magnitudes ≥ M. Parameters ***a*** and ***b***: constants; ***a***- general level of seismicity in a certain region (greater value of ***a*** implies higher seismicity), ***b***- slope of frequency-magnitude distribution; depends on the stress regime and the tectonic and structural conditions (review in Gadkari and Mukherjee 2020). It describes the number of seismic events (N) as abscissa in a log-scale and their corresponding magnitudes (M).

The b-value can be calculated either by maximum likelihood or through the linear least square regression as follows [51]:

$$b = M^{-} - \text{Mminloge} \quad (2)$$

M^{-}: mean magnitude, M_{min}: minimum magnitude of the given dataset. Generally, the minimum magnitude is obtained by plotting the cumulative number of events as a function of magnitude. This plot is then fitted with straight line and M_{min} is the level at which, data fall below the line.

4. Results

4.1. Aspect-slope differentiation & drainage-order analysis

A terrain's aspect and degree of slope are displayed on an aspect-slope map. The results of the geomorphic computations are linked with the local tectonics and slope. The aspect map indicates the direction the slope facing, which is measured clockwise from the north in degrees (Fig. 3A). Dynamically graded river channels of the eighteen watersheds were derived from the hilly patches of Tripura- Mizoram parallel fold anticlines. These rain-fed rivers with their tributaries reframed successively by tectonics and sediment aggradation with varying initiated flows. Such drainage orientations also determine the stream-order and its relation with structure. Watershed 10 possesses fifth-order stream and most of the watersheds consist of fourth-order streams. Several first-order streams join at right-angle to their higher orders in watersheds 2, 10, 12, 15 and 17. These streams have framed rectangular drainage patterns (Fig. 3B).

4.2. Spatial-scale geomorphic indices

- **Circularity Ratio (R_c)**
  The eighteen watersheds have been grouped into four classes: Class 1 (R_c = 0.113-0.183), Class 2 (R_c = 0.184-0.270), Class 3 (R_c = 0.271-0.313 3) and Class 4 (R_c = 0.314-0.395) (Supplementary Fig. 1a).
- **Drainage Texture (D_t)**
  Watershed 10 is under Class 1 (D_t = 0.654-0.972), Watersheds 2-9 and 12, 15 and 16 are under Class 2 (D_t = 0.386-0.653), four watersheds viz., 1, 5, 13 and 14 are under Class 3 (D_t = 0.306-0.385), and watersheds 11, 17 and 18 belong to Class 4 (D_t = 0.262-0.305). Results indicate that the entire area consists of course drainage structure (Supplementary Fig. 1b).
- **Hypsometric Integral (HI)**
  Higher range of HI = 0.216-0.322 indicate less erosion rate in upland hilly area of watersheds 15, 17 and 18 (Class 1), which are followed by HI = 0.171-0.215 for watersheds 1, 4, 5, 7 and 8 (Class 2), watersheds 3, 9, 14 and 16 (Class 3) with HI = 0.144-0.170 and watersheds 2, 6, 10, 11, 12 and 13 (Class 4) with HI = 0.116 to 0.143. Generally, it is suggested that less eroded basins are under the young stage as active tectonics produces rugged landscape (Hamdouni et al., 2008) (Supplementary Fig. 1c).
- **Elongation Ratio (R_e)**
  Watersheds 12 and 14-18 (Class 1) have R_e = 0.383- 0.454. R_e = 0.455-0.620 is for Class 3 watersheds 2, 3, 11 and 13. Watersheds 1, 8, 9 and 10 are under moderate tectonic activity with R_e = 0.603-0.678. Except watershed 3, 4, 5 and 7 all the fourteen watersheds are elongated with R_e < 0.7. The most elongated watersheds 3 and 4

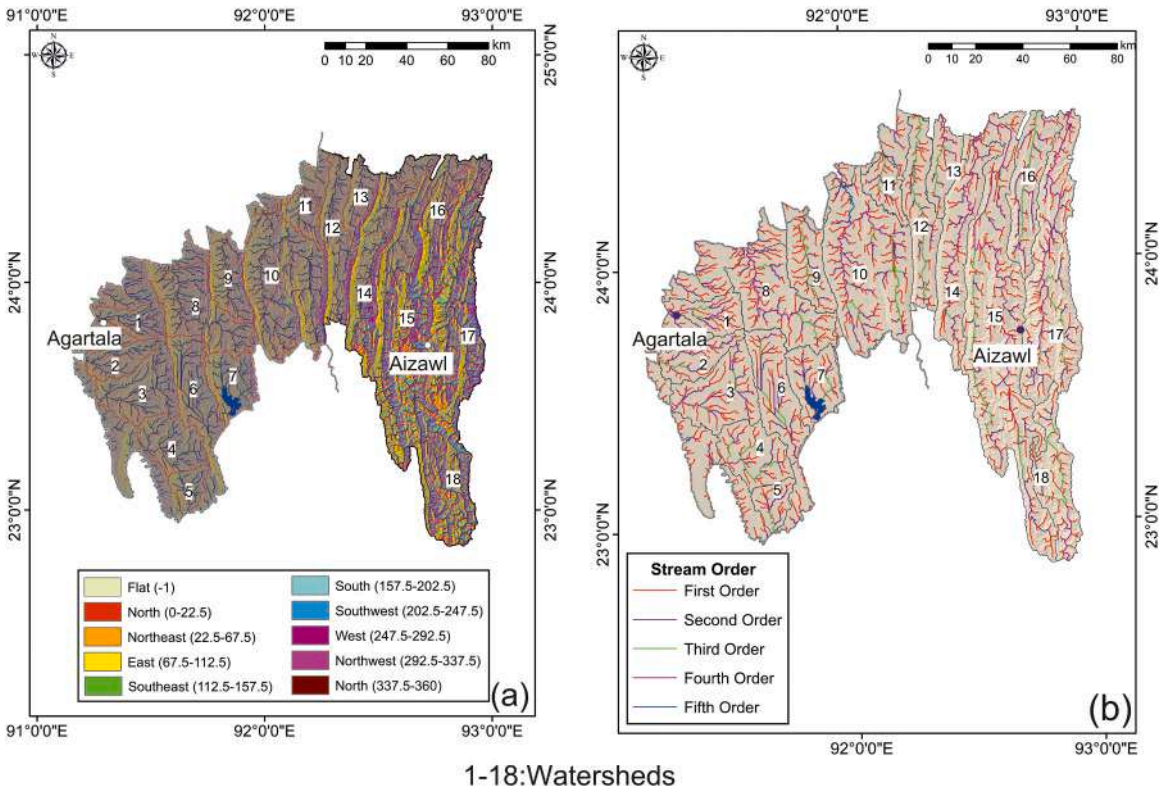

Fig. 3. a. Slope aspect map showing the direction of slope of each watershed. **b.** Map of stream order considering all tributaries of the master streams of each watershed.

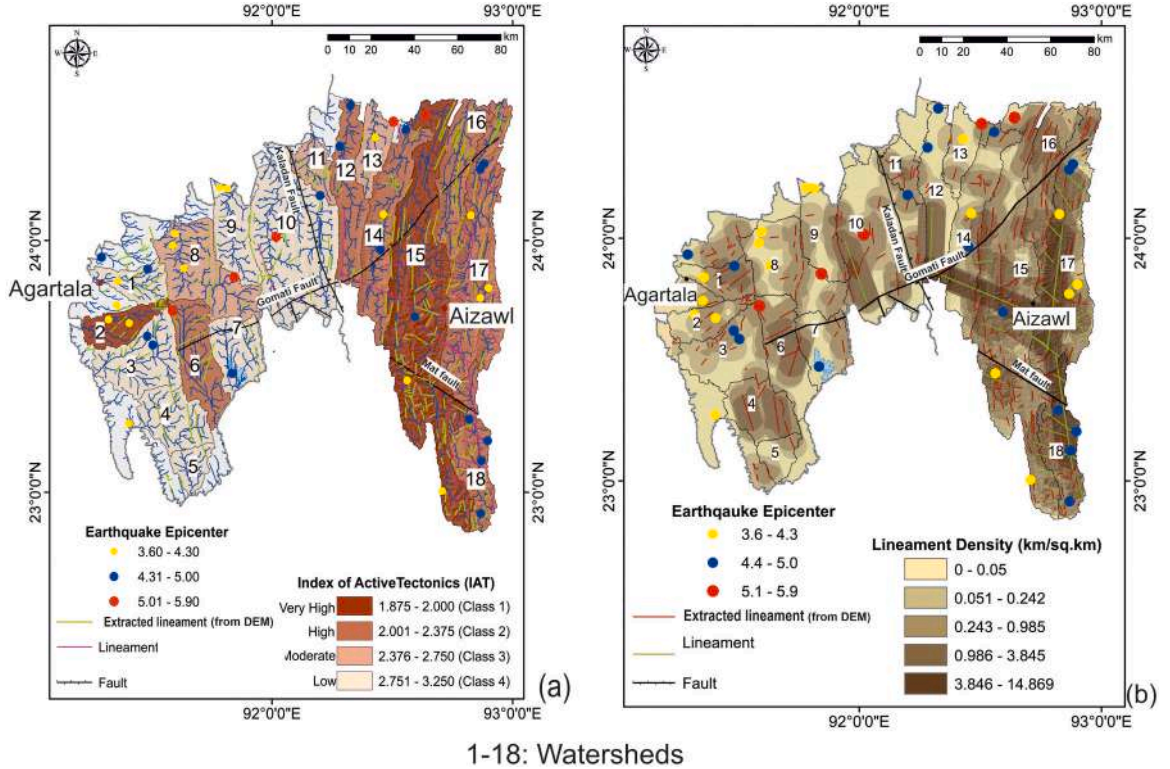

Fig. 4. a. Map of Index of Active Tectonics: Four classes- Class 1 (very high), Class 2 (high), Class 3 (moderate), and Class 4 (low). Major faults and lineaments extracted from DEM and compiled from previous literature. **b.** Lineament density map with earthquake magnitudes from 3.6–5.9 Mb.

tend to be less circular in the tectonically active area (Supplementary 1d).

- **Basin shape index (Bs)**

  High Bs = 5.548-7.510 for watersheds 14 and 17 are the places with N-S and NW-SE lineaments. These watersheds are elongated. Bs = 3.307-50547 is found for the watersheds 6, 12, 15 and 16. For watersheds 1, 2, 10,11, 13 and 18, Bs = 1.664-3.306 indicates moderate tectonic activity. Watersheds 3, 4, 5 and 7 are under Class 4 (Rf = 0.362-0.712).

- **Asymmetry Factor (AF)**

  Calculated Asymmetry Factor (AF) for the watersheds 2, 4, 10 and 15 indicate that those are more tilted tectonically (Class 1, AF = 17.161-30.655) than the watersheds 3, 5, 6, 7 and 18 (Class 2) with AF = 6.861-17.160. AF = 2.376-6.860 in watersheds 11, 12, 14 and 17 (Class 3) indicates modearate tectonic tilting. Watersheds in Class 4, viz., 1, 8 and 9 with AF = 0.004-2.376 indicate negligible tilt. Here, all the normalized AF values < 50 indicate the watersheds to be tilted towards downstream.

- **Form Factor (R_f)**

  The value of R_f = 0.115-0.162 for watersheds as 12 and 14-18 (Class-1) indicates that those are active tectonically. Watersheds 2 and 6 under class 2 (1.063-0.285). R_f = 0.286-0.361 is for Class 3 that covers watersheds 1, 8, 9 and 10. Watersheds 3, 4, 5 and 7 are under Class 4 (R_f = 0.362-0.712). Smaller the R_f, more elongated is the watershed indicating vertical incision and structural control.

- **Transverse Topographic asymmetry factor (T)**

  Calculated higher T = 0.691-0.790 for the watersheds 2 and 15 come under Class 1 (tectonically very active). T = 0.690 to 0.451 indicates high activity covering watersheds 6, 8, 11 and 12. Moderately active watersheds are 1, 3, 5 and 13 with T = 0.311-0.450 (Class 3). Watersheds 4, 7, 9, 10, 14, 16,17 and 18 belong to less active areas and under Class 4 (T = 0.210-0.310).

- **Index of Active Tectonics (IAT)**

To combine the different value ranges of individual indicators, IAT for each watershed has been estimated. IAT has been applied in comprehending the evolution of tectonic activity of the study area. Lower values of IAT indicates higher tectonic activity. The four classified ranges of IAT are 1.875–2.000 (Class 1), 2.001–2.375 (Class 2), 2.376–2.750 (Class 3) and 2.751–3.250 (Class 4). The low IAT (Class 1) indicates a significantly high tectonic activity for watersheds 1 and 15. Watersheds 6, 14, 16, 17 and 18 come under Class 2 as highly active. Tectonically the watersheds 1, 4, 11 and 12 under Class 3 are moderately active. Class 4 includes the watersheds 3, 5, 8, 9, 10 and 13 with IAT = 2.751–3.250, which are less active (Fig. 4a). According to the IAT range watershed 8 is moderately active (Fig. 4a) whereas as per the asymmetry factor analysis this watershed is under low tectonic activity (Suppl. Fig. 1h). In IAT model we normalized all the indicators in a single-scale customizing the rank of each parameter. Therefore as per the IAT range, watershed 8 is moderately active tectonically.

The spatial distribution of lineament density supports that watersheds 2, 7, 15 and 16 are highly to very highly active tectonically. The eastern section of the study area near the Mat Fault are characterized by a higher density of lineaments (Fig. 4b). The Mizoram fold belt range and the nearby region of watershed 2 experienced low to high magnitude of earthquakes. Distribution of seismic epicentres indicate that the watersheds 2, 3, 14, 15, 16, and 17 are tectonically active in parts of the Surma basin (Fig. 4b).

4.3. Linear-scale analysis

- **Meso-scale**

  Longitudinal profile is an important geomorphic tool to interpret the evolution of river undergoing various neotectonic disturbances [19,21]. In other words, a river's longitudinal profile is a key geomorphic indicator of tectonic and geologic disturbances. It is a curve with convex and concave surfaces, with a greater degree of concavity at the headwaters. The concave form of the stream profile is linked to a gradual upstream rise in stream discharge (Bull and Knuepfer, 1987). The irregularity in the profile is a result of neotectonic and tributary confluences. We analysed in detail the watersheds 2 and 15 that are highly active tectonically as per the IAT range = 1. 875-2.00. We chose 10 sections of two master streams to estimate SL and SI. The long profile curves and SLs were compared to find out the knick points. Concavity curves were plotted in a comparison with elevation (m) along the master streams of watersheds 2 and 15. At equilibrium condition, the convex-up profile is formed when the river adjusts to increasing resistance and / or decreasing discharge downstream. The concave-up profile is exhibited by river where they adjust to decreasing resistance and / or excessive increasing discharge downstream. In watershed 2 from source to mouth the channel is sinuous and display increased values of SL near the mouth (SL = 49.95 and 77.02) and in the mid-course (SL = 39.50 and 56.76) where the channel crosses the lineaments (Fig. 5a). Fig. 4b presents knick points developed in breakoff slope along the channel with high SL values (120.91). We marked the profile as 'A-B′, and the inset graph of elevation and concavity as 'A′ – B′' (Fig. 5b). This marked section displays the low concavity in the middle course and near mouth as well where high SL values have been observed (Fig. 5a).

  In watershed 15, the entire channel is sinuous and SL = 259.78 and 123.72 are drastically increased ~ 45 km downstream from the source where the channel crosses several lineaments. SL = 103.98 and 249.44 again increases near the river mouth. These alterations are due the existence of lineaments across and along the channel, the major one being the Gomati Fault (Fig. 5c). In Fig. 5d, two distinct knick points have been identified between the marked section 'A-B′. The highest SL picks exist near 'A′ where the break-off slope indicates the presence of knick point. The inset graph of elevation / concavity comparison discloses the same section marked as 'A′ - B′ where low concavity values are in the mid-course of the river as well in the lowermost part.

  The alternating low values of concavity signify the vertical incision and manifest as a convex profile. A comparative study of low concavity with low elevation between 'A-B′ denotes tectonic interferences. However, low values of concavity with less elevated sections indicate the part to be rejuvenated once. Towards mouth, it remains as a normal graphical representation with high concavity and low elevation. Concave river profiles are actually common in mid to lower part of any ideal master stream. This is observed in watersheds 2 and 15.

- **Micro-scale**

Ten micro-scale watersheds identified in Fig. 6a are processed using digitising tools. Asymmetry factor (AF) in micro scale watersheds analyse [28] are presented in Table 1. Analyses indicate watershed 1 and 7 have AF ≈ 50. Watersheds 2 and 9 show significantly lower values of AF = 28.7 and 24.94, respectively. This indicates that these watersheds are tilted towards the downstream. Watershed 6 and 8 show a little higher AF= 62.15 and 63.93, respectively, and indicate that they are tilted towards downstream. Watersheds 3 and 10 have lower values of AF= 46.23 and 46.13, respectively. This also indicates that the watersheds are tilted towards downstream.

Watersheds 1–4 and 8 have lower values of V_{fwh}, which indicate a certain degree of stream erosion. V_{fwh} values of watershed 6, 7, 9 and 10 suggest wide and low-lying terrains, which is also the case with watershed 5 in the downstream portion. Sinuosity Index (SI) [11] estimated for main streams of these 10 watersheds are presented in Fig. 6a. Streams of watershed 2, 4 and 5 have SI values > 2 suggesting moderate meandering flow. This indicates a low gradient. Streams of other watersheds with SI between 1–1.7 indicates low meandering flow. This indicates more or less straight flow controlled by ridge and lineaments

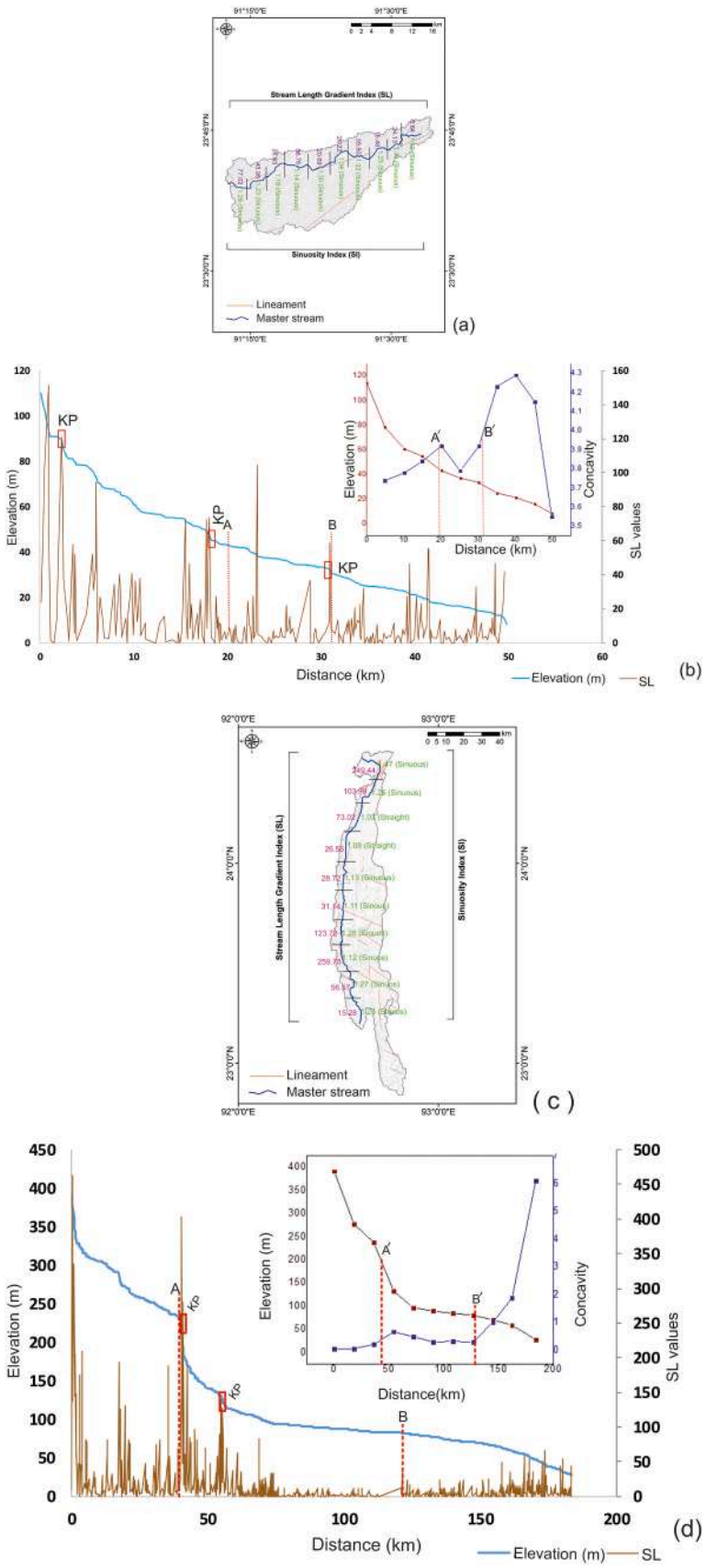

Fig. 5. a. Reach-wise SL and SI values of master streams of watershed 2. b. Elevation profile with computed SL values along the long profile of the master stream. Three knick points (KP) marked. Inset graph shows a sudden drop of concavity in the river's mid-course. c. Reach-wise SL and SI values of master streams of watershed 15. d. Two knick points (KP) marked. Inset- drop of concavity in the river's mid-course.

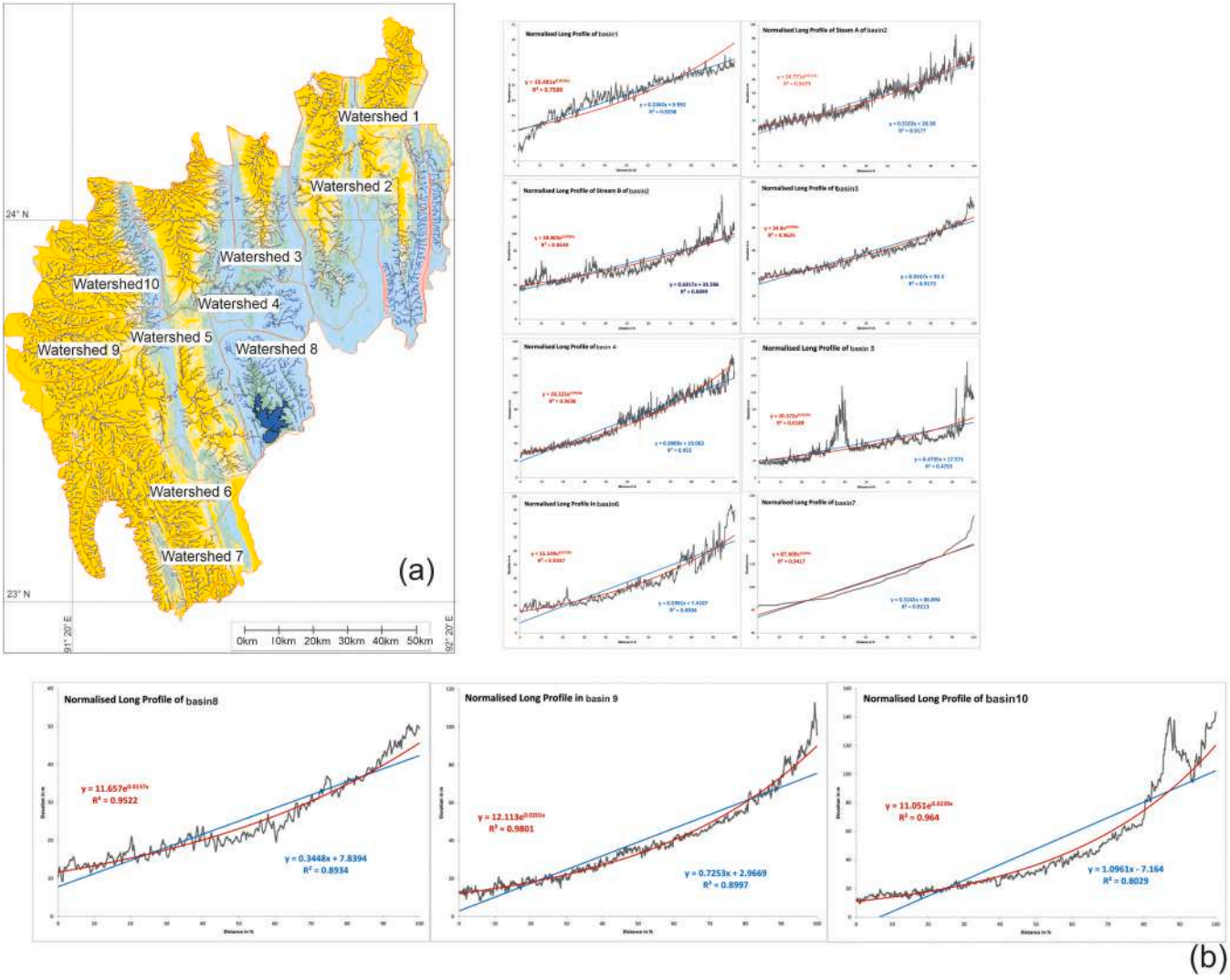

Fig. 6. a. Drainage basins prepared from visual interpretation of Landsat OLI and watershed analyses of DEM. Ten micro-basins/ watersheds considered in this study. **b.** Normalized long profiles of these watersheds.

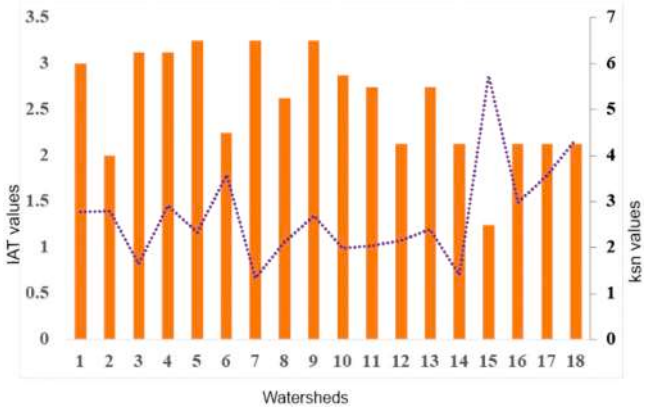

Fig. 7. Comparative graphical presentation of IAT values with steepness index (k_{sn}) for each watershed.

developed form the folded structures.

Hypsometric Curve Analyses [55] gives the idea of relative elevations of a particular percentage of area. Most of the areas in Tripura are of low elevation of < 50 m. About 85 % of the total area is under 100 m elevation. Nearly 10 % of the area are 100 to 200 m elevated. Presence of very less but significantly elevated (up to 800 m) areas are due to the N-S trending folds.

Main streams for the 10 watersheds were analysed for the normalised longitudinal profiles [30]. The profiles are fitted with linear and exponential regression curves by using standard equations y = f(x). The coefficients of correlation (R^2) are shown in Fig. 6a,b. Except watershed 5, the linear and exponential curve fits were found satisfactory as confirmed from the R^2 values. For watersheds 6, 7, 8, 9 and 10, the mid-stream segments had undergone more erosion and deposition in the downstream portion. Usually this might happen due to sudden uplift of the upstream side. In the profiles of watershed 2 and 5, ridges are truncated (Fig. 6b).

4.4. Normalized steepness index (k_{ns})

The calculated steepness index (k_{ns}) values have been compared to justify the IAT rank. When compared to its drainage area, a channel's unexpected steepness or mild slope are indicated by the steepness index. Channel gradients should decline as the drainage-watershed area increases. The steepness of the eighteen watersheds has been calculated and presented along with each watershed's specific IAT value in a comparative graph. It indicates that watershed 2 and 15 consist of high

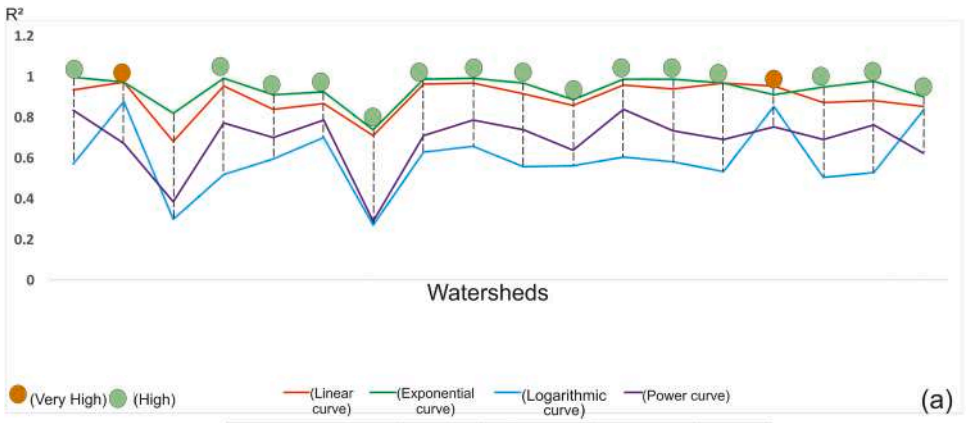

Watersheds	Linear $_{(R^2)}$	Exponential$_{(R^2)}$	Logarithmic$_{(R^2)}$	Power$_{(R^2)}$
1	0.9325	0.9951	0.5692	0.8324
2	0.9716	0.9715	0.8777	0.6741
3	0.6805	0.8178	0.2972	0.386
4	0.9541	0.9941	0.5204	0.7722
5	0.8391	0.9099	0.5955	0.7023
6	0.8693	0.923	0.7018	0.7863
7	0.7123	0.7386	0.2704	0.2919
8	0.964	0.9855	0.6282	0.7086
9	0.9661	0.9917	0.6574	0.787
10	0.9143	0.9687	0.5549	0.7406
11	0.8579	0.889	0.5639	0.6382
12	0.9584	0.9875	0.6049	0.8389
13	0.9387	0.9854	0.5799	0.736
14	0.9683	0.9693	0.5328	0.6888
15	0.9555	0.9096	0.8535	0.7547
16	0.8706	0.9483	0.5069	0.6887
17	0.8843	0.9784	0.5279	0.7633
18	0.8552	0.9003	0.8319	0.6246

(b)

Fig. 8. a. Line graph of four calculated best-fit curves as linear, exponential, logarithmic and power. **b.** Calculations of linear, exponential, logarithmic and power curve-fit.

steepness values as well a low IAT indicating very active tectonics (Fig. 7).

4.5. Best-fit curve analysis & tectonic assessment

The long profiles of the river reflect the changes in the relief and extent of the watershed. The long-profile length and relief are thus normalized in order to reduce the effects of the watershed size and relief. To normalize in this way, the elevations and distances were divided by the head (maximum watershed relief) and the overall stream length, respectively [30]. Breaks in the river profile therefore indicate a significant structural influence on the river course. The R^2 value determines the best fit. The curve with the highest R^2 value is the best fit curve. As per Lee & Tsai [30], when channel grain size exceeds the river's transportation capacity, the long profile exhibits a low degree of concavity, which results in a better fit for a linear function. According to Hack [19], when erosion balances resistance, the grain size of the channel sediment decreases downstream, making the long profile closer to the log function. This is the river's "graded profile". The power function is increasingly suitable as the profile concavity increases. Therefore, the order of evolution should be linear, exponential, logarithmic, and power curve. Fig. 8a presents linear, exponential, logarithmic, and power curves with a comparative visualization of tectonically very high watersheds. The curves display the highest R^2 values in linear curve fit of watersheds 2 and 15 that denote very high tectonic activity. The remainder 16 watersheds are also tectonically highly active (Fig. 8b).

5. Discussions

All the spatial and linear aspects of morphometric parameters signify that the Tripura-Mizoram fold belt is tectonically active. The 2020 Champhai earthquake [1] originated in the watershed 15. The aftershock persisted for around 60 days, and Mizoram and nearby areas underwent more than six strongly felt Mw 4.0 quakes [5]. These earthquakes took place along the NW-SE-trending active Mat River Fault at shallow depths (~ <20 km). The computation of IAT in watershed-scale has been justified by the linear indicators and the steepness index. The geomorphic significance is assessed in micro-scale study where potential knick point sites are marked and are incorporated by plotting known faults and lineaments along and across the consequent channel of each watershed. The points of intersections of channels with faults and lineaments indicate the tectonic disturbances with the formation of possible structural knick points where rejuvenation occurred due to upliftment, tilting and incision mechanism. The formations of watersheds are influenced by tectonically active zones. Stream patterns can disclose active tectonics ([28]. Accordingly, these drainage networks reflect how topographic features have changed over time. Flexure or warping of a portion of the topography reflects tilting of watersheds. Values of basin asymmetry factor between the range of 17.16–30.655 (Class-1), tilted towards NW and SE with more area on single sides of the watersheds (2, 4, 10 and 15). The tilting of the watersheds is the same as those of the asymmetric anticlines of the Tripura –Mizoram fold belt.

All factors, such as rock of different hardness, development of subsequent tributaries, neotectonic movements and discontinuities causing different stages are considered in the evolution of the profile. Watersheds 2 and 15 are tectonically highly active. In total, morphometric indicators explain the channel behaviour, lineament density, incision, curvature, length/gradient alteration, earthquake magnitudes and overall steepness of each watershed that strongly support the active

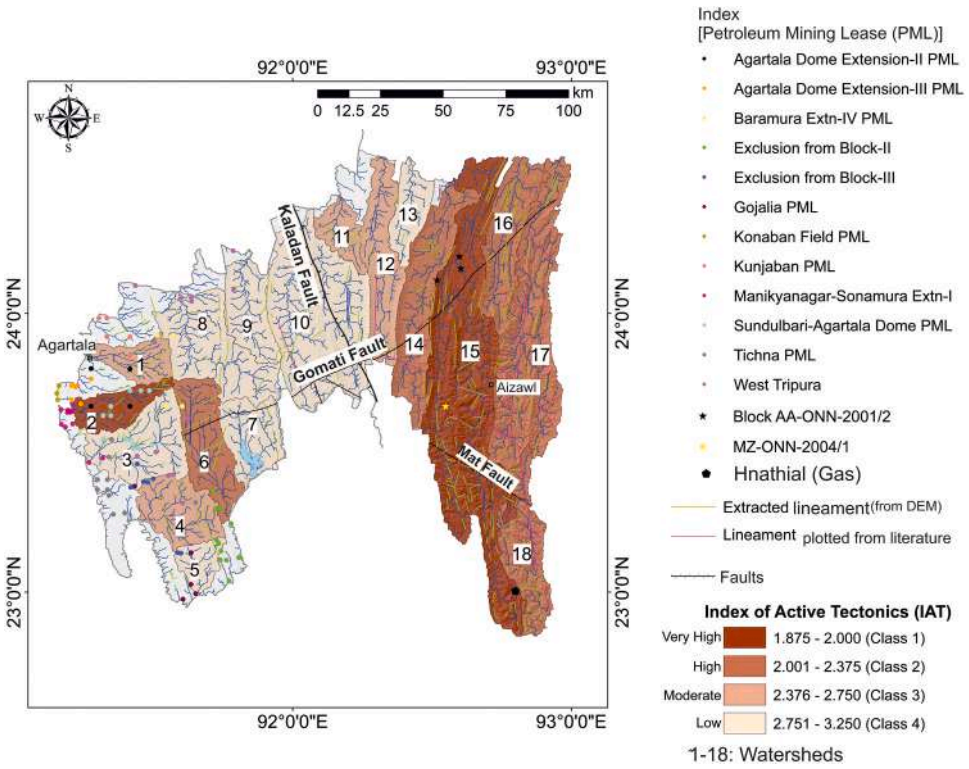

Fig. 9. Distribution of petroleum mining lease (PML) sites. A gas extraction site (Hnathial) plotted. Most of the PML sites are located within watershed 2, 3 and 15.

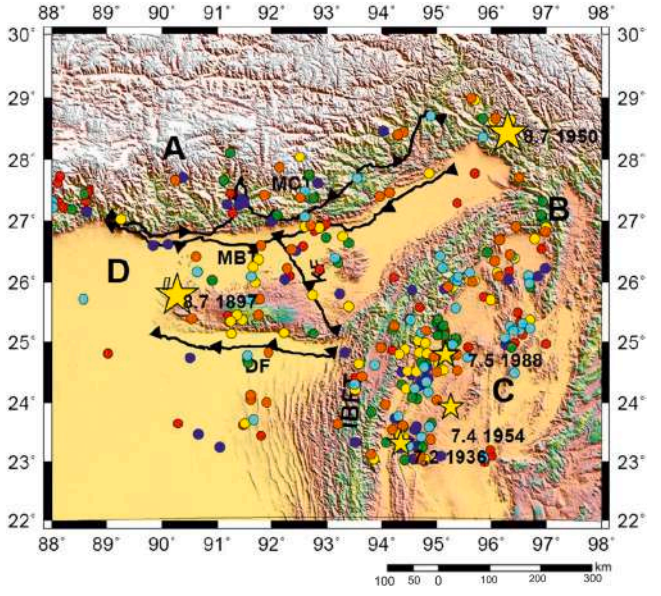

Fig. 10. Spatial distribution of seismic events from 1969–2012 in six time period of four blocks as per Ray et al. (2014). First period (orange): 29-Sept-1969 to 21-Aug-1972, second period (cyan) 21-Aug-1972 to 7-Dec-1974, third period (yellow) 06-July-1982 to 16-Sept-1984, fourth period (green) 15-Feb-1987 to 8-March-1989, fifth period (blue colour) 04-Oct-1992 to 03-Msrch-1993 and sixth period (red colour) 23-June-2011 to 11-Nov-2012 (Roy et al., 2014).

tectonics. In watershed 2, lineaments trend E-W. The Tripura fold belt is composed of several long narrow anticlines with N-S axial traces and are separated by board intervening synclines that control the drainage alignment and watershed shapes. Offsets are reported in a few of these anticlines [10]. Watershed 15's lineaments are N-S aligned as the watershed developed along a fold. Gomati and Mat faults running across the fold justify the watershed to be under the very high range of IAT.

This work utilizes IAT to evaluate and categorize the watersheds. Major faults- The Gomti Fault and the Mat Fault passes through the terrain of Bhatterchajee (1991). This indicates that the watersheds are tectonically active.

We evaluate eight morphometric indicators in basin-scale. Overall the Mizoram section is deformed by smaller-scale isoclinal jointed folds with steep axial planes and horizontal to gently plunging axes that justify the recent tectonic activity [9]. Watersheds 2 and 15 are highly active tectonically as they fall in Class 1 in the IAT range. Bhatterchajee (1991) mentioned that there are three distinct types of faults in the Tripura-Mizoram fold belt.

With an increase in uplift rate and a decrease in erodibility, the steepness index rises, which is accompanied by episodic tectonic disturbances. Locations of petroleum mining lease (PML) indicate that the western section of Surma Basin- the Tripura anticline section and near watershed 15 the north of Aizawl are the zones of interest for petroleum geoscience (Fig. 9). Seismic risk (Fig. 10) in this area can lead to major earthquake. Over a period of years, the precursory decline in b-value before major seismic events, such as main shock, strain hardening, aftershocks and co-seismic rupture. After the main-shock, the b-value usually rises drastically. Slip rates of 20 mm y^{-1} and 5 mm y^{-1} were reported from the Mat Fault in watersheds 15, 16 and 17 (Fig. 11).

6. Conclusions

The Tripura-Mizoram fold belt is analysed morphometrically in terms of 18 watersheds and was found to be tectonically active. In these watersheds, parallel to rectangular drainage patterns and dissected parallel anticline and syncline sequences are observed. Watersheds 2 and 15 are most active tectonically where channels are parallel to the lineaments. Watershed 15 is characterized by two major faults- the Gomati Fault and the Mat Fault. The later fault's geomorphic fingerprints indicates tectonic activity. There have been a fewer earthquakes in the last half century from the Tripura-Mizoram fold belt. Mat Fault's

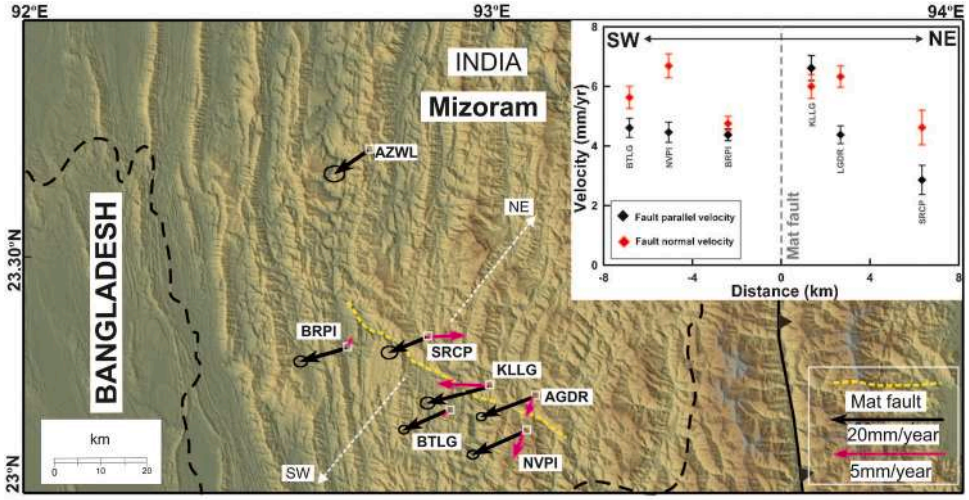

Fig. 11. Site velocity with respect to AZWL (a GPS location) and the Indian standard frame (black arrows, different scale) [53].

activity led to the 2020 Champhai earthquake in watershed 15. The high b-value indicates less numerous seismicity in watersheds 3, 4 and 9. On other hand, a low b-value indicates significant seismicity in and around watersheds, 2, 14 and 15. Well-bore stability issue in these tectonically active watersheds needs to be addressed.

Abbreviations

AF	Asymmetry Factor
ANSS	Advanced National Seismic System
DEM	Digital Elevation Model
FMD	Frequency-Magnitude Distribution
GIS	Geographic Information System
GPS	Global Positioning System
HI	Hypsometric Integral
IAT	Index of active tectonics
IRIS	International Seismological Centre
KP	Knick points
NRSC	National Remote Sensing Centre
OLI	Operational Land Imager
PML	Petroleum mining lease
SRTM	Shuttle Radar Topography Mission
USGS	United States Geological Survey
Symbols	
B_s	Basin shape Index
D_t	Drainage Texture
R_c	Circularity Ratio
R_e	Elongation Ratio
R_f	Form Factor
T	Transverse Topographic Symmetry

CRediT authorship contribution statement

Mery Biswas: Writing – original draft, Formal analysis, Conceptualization. **Soumyajit Mukherjee:** Writing – review & editing, Investigation, Funding acquisition, Conceptualization. **Manash Pratim Gogoi:** Formal analysis. **Nabanita Barik:** Writing – original draft, Investigation, Formal analysis.

Declaration of Competing Interest

Authors have no conflict of interest with anyone regarding this work.

Data Availability

Data will be made available on request.

Acknowledgements

CPDA grant (IIT Bombay) supported SM. MB thanks the Department of Geography, Presidency University, Kolkata. Dr. Yuhong He (Chief Editor) is thanked for providing detail review comments obtained from two anonymous reviewers.

Appendix A. Supporting information

Supplementary data associated with this article can be found in the online version at doi:10.1016/j.geomat.2024.100019.

References

[1] B.K. Bansal, A.K. Sutar, M. Verma, The 2020 earthquake sequence and seismic hazard scenario of Mizoram state in northeast India, Front. Earth Sci. 10 (2022) 985394.
[2] B.K. Barman, K.S. Rao, Zohmingliani, N.S. Prasad, D. Walia, Significance of neotectonics in assessing the relative tectonic activity in and around the Mat Fault of Eastern Himalayan Fold Belt, Mizoram, north-east India, Geol. J. 57 (2022) 5345–5360.
[3] Baruah, R.M., Datta, K., Murthy, M.S., 1996. Biofacies, lithofacies and depositional environment of sub-surface Surma sediments in Cacharea, Assam. In: Pandey, J., Azmi, R.J., Bhandari, A. and Dave, A., (Eds.), XV Indian Colloquium on Micropaleontology and Stratigraphy, Dehradun, 305–316.
[4] R.M. Baruah, N.P. Singh, D.C. Rao, Foraminiferal biostratigraphy of Disang and Barail groups of a part of Nagaland. Proceedings of the National Seminar on Tertiary Orogeny, 1987, pp. 305–327.
[5] B. Bharali, R. Rakshit, L. Dinpuia, S. Saikia, S. Baruah, The 2020 Mw 5.5 Mizoram earthquake and associated swarm activity in the junction of the Surma Basin and Indo-Myanmar Subduction Region, Nat. Hazards 109 (2021) 2381–2398.
[6] A.S. Bhaskar, Binoj, R.B. Kumar, Remote sensing of coastal geomorphology to understand river migration in the Thengapatnam area, southern India, Int J. Remote Sens 32 (2011) 5287–5301.
[7] M. Biswas, M.P. Gogoi, B. Mondal, T. Sivasankar, S. Mukherjee, S. Dasgupta, Geomorphic assessment of active tectonics in Jaisalmer basin (western Rajasthan, India), Geocarto Int. 37 (2022) 12382–12413.
[8] M. Biswas, M.K. Puniya, M.P. Gogoi, S. Dasgupta, S. Mukherjee, N.R. Kar, Morphotectonic analysis of petroliferous Barmer rift basin (Rajasthan, India), J. Earth Syst. Sci. 131 (2022) 140.
[9] J. Blick, R. Verma, Classification of Tlangnuam Landslide, Aizawl, Mizoram, Asian Acad. Res. J. (2018) 221–234 (URL), ⟨https://www.researchgate.net/publication/335501753_Classification_of_Tlangnuam_Landslide_Aizawl_Mizoram⟩.
[10] J. Brahma, A. Sircar, G.P. Karmakar, Pre-drill pore pressure prediction using seismic velocities data on flank and synclinal part of Atharamura anticline in the Eastern Tripura, India, J. Pet. Explor. Prod. Technol. 3 (2013) 93–103.
[11] Brice, J.C., 1964. Channel Patterns and Terraces of the Loup River in Nebraska. Geological Survey Professional Paper 422-D, Washington, D2 – D41.
[12] W.B. Bull, L.D. McFadden, Tectonic geomorphology north and south of the Garlock fault, California. Geomorphology in Arid Regions, in: D.O. Doehring (Ed.), Proceedings of the Eight Annual Geomorphology Symposium, State University of New York at Binghamton, Binghamton, NY, 1977, pp. 115–138.

[13] A. Das, S. Bose, S. Dasgupta, S. Roy, B. Mukhopadhyay, Post-Oligocene evolution of Indo-Burma wedge: Insights from deformation structures of Tripura Mizoram fold belt, J. Struct. Geol. 154 (2022) 104497.
[14] S. Dey, S. Paul, P. Sarkar, Morphological and microstructural evidences of paleo-seisminc occurrences in an earthquake prone zone of Tripura, India J. Earth Sci. 25 (2014) 289–298.
[15] A.K. Dwivedi, Petroleum exploration in India–a perspective and endeavours, Proc. Indian Natl. Sci. Acad. 82 (2016) 881–903.
[16] F.D. Eckardt, Geomorphology from Earth Orbit 1957-2000, in: T.P. Burt, A. S. Goudie, H.A. Viles (Eds.), The history of the study of landforms or the development of geomorphology. Vol. 5. Geomorphology in the second half of the twentieth century, Geological Society, London, 2022, pp. 19–30.
[17] S. Ganguly, Tectonic Evolution of the Mizo hills: Bull, Geol. Min. Met. Soc. India 48 (1975) 30–39.
[18] M.P. Gogoi, B. Gogoi, S. Mukherjee, Tectonic instability of the petroliferous upper Assam valley (NE India): A geomorphic approach, J. Earth Syst. Sci. 131 (2022) 18.
[19] J.T. Hack, Stream profile analysis and stream gradient index, U. S. Geol. Surv. J. Res. 1 (1973) 421–429.
[20] D. Hazrika, R. Kayal, Recent felt earthquakes (Mw 5.0–5.9) in Mizoram of north-east India region: Seismotectonics and precursor appraisal, Geol. J. 57 (2021) 877–885.
[21] J. Holbrook, S.A. Schumm, Geomorphic and sedimentary response of rivers to tectonic deformation: a brief review and critique of a tool for recognizing subtle epiorogenic deformation in modern and ancient settings, Tectonophysics v.305 (1999) 287–306.
[22] R.E. Horton, Drainage basin characteristics, Trans. Am. Geophys. Union v.13 (1932) 350–361.
[23] R.E. Horton, Erosional development of streams and their drainage basins: hydrophysical approach to quantitative morphology, Bull. Geol. Soc. Am. 56 (1945) 275–370.
[24] S. Ibotombi, M.P. Singh, Analysis of drainage systems of Manipur and implications on the tectonic evolution of Indo-Mayanmar ranges, in: P.S. Saklani (Ed.), Himalaya (Geological Aspects), Vol. 4, Satish Serial Publishing House, Delhi, 2006, pp. 285–311.
[25] H.P. Jaishi, S. Singh, R.P. Tiwari, R.C. Tiwari, Radon and thoron anomalies along Mat fault in Mizoram, India, J. Earth Syst. Sci. 122 (2013) 1507–1513.
[26] H.P. Jaishi, S. Singh, R.P. Tiwari, R.C. Tiwari, Temporal variation of soil radon and thoron concentrations in Mizoram (India), associated with earthquakes, Nat. Hazards 72 (2014) 443–454.
[27] Jena, A.K., Haldia, B.S., Solomon, R., Sahoo, A.K., Bhanja, A.K., & Samanta, A., 2012. Exploration strategy in Tripura Fold Belt, Assam & Assam Arakan Basin, India–some contemporary approach. In 9th Biennial International Conference and Exposition on Petroleum Geophysics, Hyderabad. pp. 1–8.
[28] E.A. Keller, N. Pinter, Active Tectonics: Earthquakes, Uplift and Landscape, Prentice Hall,, New Jersey, 2002.
[29] G.C. Kothyari, R.K. Dumka, K. Luirei, R.S. Kandregula, A.K. Taloor, K. Malik, A. Joshi, A.K. Patidar, U. Bhan, Estimation of active surface deformation using PSInSAR technique of the Central Himalayan region, Geocarto Int. 39 (2024) 2302415.
[30] C. Lee, L.L. Tsai, A quantitative analysis for geomorphic indices of longitudinal 809 river profile: A case study of the Choushui River, Central Taiwan, Env. Earth Sci. 59 (2009).
[31] K. Lokho, K. Kumar, Fossil pteropods (Thecosomata, holoplanktonic Mollusca) from the Eocene of Assam-Arakan Basin, north-eastern India, Curr. Sci. 94 (2008) 647–652.
[32] K. Lokho, D.S.N. Raju, Langhian (earlyMiddleMio-cene) foraminiferal assemblage from Bhuban Formation, Mizoram, NE India, J. Geol. Soc. India 70 (2007) 933–938.
[33] K. Lokho, R.K. Saxena, D.S.N. Raju, A. Kumar, Middle Miocene calcareous nannofossils from the Upper Bhuban Formation of Mizoram, Indo-Burma Range, Micropaleontology 62 (2016) 341–352.
[34] S.A. Mahmood, R. Gloaguen, Appraisal of active tectonics in Hindu Kush: Insights from DEM derived geomorphic indices and drainage analysis, Geosci. Front. 3 (2012) 407–428.
[35] J. Malsawma, P. Lalnuntluanga, S. Sailo, V. Vanthangliana, R.P. Tiwari, V. K. Gahalaut, The 22 June 2020 Mizoram, India earthquake (Mw 5.5): an unusual intra-wedge shallow earthquake in the Indo-Burmese Wedge, Curr. Sci. 120 (2021) 1514.
[36] N. Manchar, R. Hadji, A. Bougherara, K. Boufaa, Assessment of relative-active tectonics in Rhumel-Smendou basin (NE Algeria) – observations from the morphometric indices and hydrographic features obtained by the digital elevation model, Geomat., Land Manag. Landsc. (2022) 47–66.
[37] S. Mitra, K. Priestley, A.K. Bhattacharyya, V.K. Gaur, Crustal structure and earthquake focal depths beneath northeastern India and southern Tibet, Geophys. J. Int. 160 (2005) 227–248.
[38] D.R. Nandy, Geodynamics of northeastern Indian and the adjoining region, ACB Publications,, Kolkata, 2001.
[39] P.K. Rai, R.C. Chandel, V.N. Mishra, P. Singh, Hydrological Inferences through Morphometric Analysis of Lower Kosi River Basin of India for Water Resource Management based on Remote Sensing Data, Appl. Water Sci. 8-15 (2018) 1–16.
[40] R. Rakshit, D. Bezbaruah, F. Zaman, B. Bharali, S. Saikia, Locked crustal faults associated with the subducting Indian Lithosphere and its implications in seismotectonic activity in the Central Indo-Burmese Ranges, Northeast India, Geofizika 39 (2022) 1–18.
[41] R. Rakshit, D. Bezbaruah, Morphotectonic aspects in and around Aizawl, Mizoram of NE India, South East Asian J. Sediment. Basin Res. 2-3-4 (2016) 28–36.
[42] S. Singh, A. Guha, V. K. Kumar, S. Bardhan, A. Lesslie, K.V. Kumar, A. Chatterjeee, Satellite based mapping and morphogenetic analysis of the landforms in the tertiary fold belts of parts of Tripura, India, Geocarto Int. 30 (9) (2015) 1–31.
[43] S. Singh, H. Prasad Jaishi, R. Prasad Tiwari, R. Chandra Tiwari, Variations of soil radon concentrations along Chite Fault in Aizawl district, Mizoram, India, Radiat. Prot. Dosim. 162 (1-2) (2014) 73–77.
[44] M.J. Smith, J. Mike, P.P. Smith, S.G. James, Chapter Eight–Digital Mapping: visualisation. Interpretation and Quantification of Landforms, in: M.J. Smith, P. Paron, J.S. Griffiths (Eds.), Developments in Earth Surface Processes, Elsevier, London, 2012, pp. 225–251.
[45] A.N. Strahler, Hypsometric (area-altitude) analysis of erosional topography, Geol. Soc. Am. Bull. 63 (1952) 1117–1142.
[46] M.A. Summerfield, Plate tectonics and macrogeomorphology, in: T.P. Burt, A. S. Goudie, H.A. Viles (Eds.), The history of the study of landforms or the development of geomorphology. Vol. 5. Geomorphology in the second half of the twentieth century, Geological Society, London, Memoir 58, 2022, pp. 73–85.
[47] H. Taib, R. Hadji, Y. Hamed, M. Gentilucci, K. Badri, Integrated geospatial analysis for identifying regions of active tectonics in the Saharian Atlas, an review analysis of methodology and calculation fundamentals, J. Afr. Earth Sci. 211 (2024) 105188.
[48] A.K. Taloor, R. Sharma, G.C. Kothyari, Tectono-geomorphic and active deformation studies in the Ujh basin of Northwestern Himalaya, Quat. Sci. Adv. 12 (2023) 100121.
[49] A.K. Taloor, S. Sharma, J. Jamwal, S. Kumar, Quantitative and qualitative study of the Tawi basin: Inferences from Digital Elevation Model (DEM) using geospatial technology, Quat. Sci. Adv. 14 (2024) 100182.
[50] D. Theler, E. Reynard, E. Bardou, Assessing sediment dynamics from geomorphological maps: Bruchi torrential system, Swiss Alps. J Maps 4 (2008) 277–289.
[51] K.K.S. Thingbaijam, S.K. Nath, A. Yadav, A. Raj, M.Y. Walling, W.K. Mohanty, Recent seismicity in Northeast India and its adjoining region, J. Seismol. 12 (2008) 107–123.
[52] T. Thuamthansanga, R.C. Tiwari, Correlation of in-situ online 222Rn data at Mat fault with geophysical process, Mater. Today.: Proc. 65 (2022) 2825–2831.
[53] R.P. Tiwari, V.K. Gahalaut, C.U. Rao, C. Lalsawta, B. Kundu, Malsawmtluanga, No evidence for shallow shear motion on the Mat Fault, a prominent strike slip fault in the Indo-Burmese wedge, J. Earth Syst. Sci. 124 (2015) 1039–1046.
[54] Yang, X., Damen, M.C.J., Van Zuidam, R.A., 1999. Use of Thematic Mapper imagery with a geographic information system for geomorphologic mapping in a large deltaic lowland,
[55] I. Zăvoianu, Hypsometric curves and longitudinal stream profiles, Ed. Dev. Water Sci. 20 (1985) 185–200.